

Semi-Supervised Conformal Prediction With Unlabeled Nonconformity Score

Xuanning Zhou^{1,2*}, Hao Zeng¹, Xiaobo Xia³, Bingyi Jing¹, Hongxin Wei[†]

¹Southern University of Science and Technology

²Harbin Institute of Technology, Shenzhen

³National University of Singapore

Abstract

Conformal prediction (CP) is a powerful framework for uncertainty quantification, providing prediction sets with coverage guarantees when calibrated on sufficient labeled data. However, in real-world applications where labeled data is often limited, standard CP can lead to coverage deviation and output overly large prediction sets. In this paper, we extend CP to the semi-supervised setting and propose *SemiCP*, leveraging both labeled data and unlabeled data for calibration. Specifically, we introduce a novel nonconformity score function, *NNM*, designed for unlabeled data. This function selects labeled data with similar pseudo-label scores to estimate nonconformity scores, integrating them into the calibration process to overcome sample size limitations. We theoretically demonstrate that, under mild assumptions, *SemiCP* provide asymptotically coverage guarantee for prediction sets. Extensive experiments further validate that our approach effectively reduces instability and inefficiency under limited calibration data, can be adapted to conditional coverage settings, and integrates seamlessly with existing CP methods.

1 Introduction

Uncertainty estimation is crucial for safe deployment of machine learning models, particularly in high-stakes applications such as financial decision-making (Cresswell et al., 2024; Vovk and Bendtsen, 2018) and medical diagnostics (Vazquez and Facelli, 2022; Olsson et al., 2022). This necessity highlights the utility of Conformal Prediction (CP), a statistical framework that yields prediction sets containing ground-truth labels with a desired coverage guarantee (Vovk et al., 2005; Shafer and Vovk, 2008; Angelopoulos and Bates, 2021). In particular, smaller *valid* prediction sets indicate lower uncertainty in the predictions and vice versa. In this manner, conformal prediction can communicate the degree of trustworthiness without any assumptions on the model’s correctness.

Split conformal prediction (Papadopoulos et al., 2002; Lei et al., 2018), the most widely used CP framework, employs a hold-out labeled set to calibrate the threshold for prediction set construction. While computationally efficient, this framework suffers from overly conservative prediction sets with high variability when labeled data is limited (see Figure 1) (Linusson et al., 2014; Ding et al., 2024). To alleviate this issue, previous works attempt to interpolate calibration instances or use modified p-value definitions, but they are heuristic and fail to provide finite-sample guarantees (Johansson et al., 2015; Carlsson et al., 2015). Besides, few-shot CP (Fisch et al., 2021) employs a meta-learning approach using similar auxiliary tasks, but its dependence on exchangeable task collections limits practicality. This motivates us to explore another alternative - leveraging unlabelled data to address the data-scarce problem in the labeled calibration set.

*Work done while working at SUSTech as a visiting scholar.

[†]Corresponding author: Hongxin Wei (weihx@sustech.edu.cn).

In this work, we propose *Semi-Supervised Conformal Prediction (SemiCP)*, which utilizes both labeled and unlabeled data in the calibration process of split conformal prediction. In Proposition 1, we show theoretically that, assuming an accurate estimate of the nonconformity score distribution for unlabeled samples, SemiCP retains the usual coverage guarantees for its prediction sets. To this end, we design a novel nonconformity score function for unlabeled data – *Nearest Neighbor Matching (dubbed NNM)*. For each unlabeled example, we locate its nearest neighbor in the labeled set by comparing their pseudo-label nonconformity scores, compute a *pseudo bias* as the difference between the neighbor’s true-label score and its pseudo-label score, and then adjust the unlabeled example’s pseudo-label score by this bias. We further theoretically prove that our estimated unlabeled score asymptotically converges to the true nonconformity score in distribution. In this manner, SemiCP with the NNM score enables the exploitation of unlabeled data for split conformal prediction.

To validate the effectiveness of our method, we conduct extensive experiments on three benchmark image classification datasets: CIFAR-10, CIFAR-100 (Krizhevsky and Hinton, 2009), and ImageNet (Deng et al., 2009). First, we empirically show that our method consistently enhances the stability and efficiency of existing scoring functions, including THR (Sadinle et al., 2019), APS (Romano et al., 2020), and RAPS (Angelopoulos et al., 2020). For example, on CIFAR-10 with 20 labeled data, SemiCP narrowed the coverage gap by 76% and the prediction set size by 7%. In addition, SemiCP enhances conformal prediction performance across varying amounts of unlabeled data, achieving benefits with as few as 10 examples. Moreover, our SemiCP can be effectively applied to conditional CP (Papadopoulos et al., 2002; Vovk et al., 2005) and integrated with other CP algorithms (such as ClusterCP (Ding et al., 2024)). Finally, our SemiCP achieves the improvements on 10 different models, highlighting its model-agnostic nature. In summary, these results collectively demonstrate the effectiveness, scalability, and broad applicability of the SemiCP for reliable uncertainty quantification.

We summarize our contributions as follows:

- We propose a semi-supervised conformal prediction framework with an unlabeled nonconformity score for unlabeled data. Our method is complementary to existing score functions and can be extended to conditional conformal prediction.
- We theoretically prove that the estimated nonconformity scores asymptotically converge to the true scores in distribution, ensuring the coverage guarantee in the semi-supervised setting.
- We conduct extensive experiments to validate the effectiveness and applicability of the proposed method. Besides, our method is data-efficient and model-agnostic. We also provide ablation studies to show the advantages of the proposed method in Appendix H.

2 Preliminaries

Conformal prediction (CP) (Vovk et al., 2005) aims to produce prediction sets that contain ground-truth labels with a desired coverage rate. Let $\mathcal{P}_{\mathcal{X}\mathcal{Y}}$ denote the joint distribution over inputs and labels, where $\mathcal{X} \subset \mathbb{R}^d$ denotes the input space and $\mathcal{Y} \subset \{1, \dots, K\}$ denotes the label space in multi-class classification. Formally, the goal of conformal prediction is to construct a set-valued mapping $\mathcal{C} : \mathcal{X} \rightarrow 2^{\mathcal{Y}}$ that satisfies the marginal coverage:

$$\mathbb{P}(y \in \mathcal{C}_{1-\alpha}(\mathbf{x})) \geq 1 - \alpha, \quad (1)$$

for a user-defined miscoverage level $\alpha \in (0, 1)$, where input $\mathbf{x} \in \mathcal{X}$ and output $y \in \mathcal{Y}$. For conditional coverage, the goal is then to satisfy $\mathbb{P}(y_{\text{test}} \in \mathcal{C}_{1-\alpha}(\mathbf{x}) | \mathbf{x} \in G_i) \geq 1 - \alpha, \forall G_i \in \mathcal{G}$, where $G_i \in \mathcal{G}$ denotes predefined subgroups.

As a popular CP framework, split conformal prediction (Shafer and Vovk, 2008) introduces a hold-out calibration set $\mathcal{D}_{\text{cal}} = \{(\mathbf{x}_i, y_i)\}_{i=1}^n$ consisting of labeled examples i.i.d. drawn from $\mathcal{P}_{\mathcal{X}\mathcal{Y}}$. For each example (\mathbf{x}_i, y_i) from the calibration set, we calculate the nonconformity score $s_i = S(\mathbf{x}_i, y_i)$ with a score function $S : \mathcal{X} \times \mathcal{Y} \rightarrow \mathbb{R}$, which quantifies how nonconforming a data point is. For $q \in [0, 1]$ and a finite set $A \subseteq \mathbb{R}$, let $\text{Quantile}(A, q)$ denote the smallest $a \in A$ such that q fraction of elements in A are less than or equal to a . Then, we obtain a threshold as:

$$\hat{\tau} = \text{Quantile}(\{s_i\}_{i=1}^n, \frac{\lceil (n+1)(1-\alpha) \rceil}{n}). \quad (2)$$

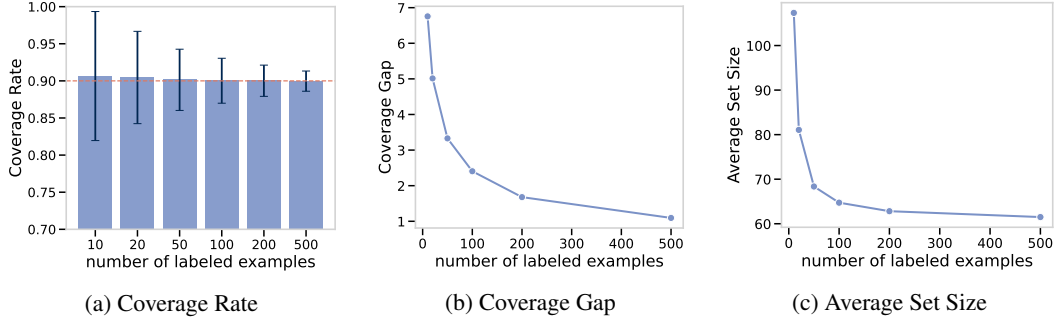


Figure 1: Impact of limited labeled data on conformal prediction, evaluated on ImageNet and ResNet50 averaged over three score functions and 100 trials.

Given a test instance \mathbf{x}_{test} , we compute the nonconformity score for each label $y \in \mathcal{Y}$ and construct the prediction set with threshold $\hat{\tau}$ as

$$\mathcal{C}_{1-\alpha}(\mathbf{x}_{\text{test}}; \hat{\tau}) := \{y \in \mathcal{Y} : S(\mathbf{x}_{\text{test}}, y) \leq \hat{\tau}\}.$$

The obtained prediction set $\mathcal{C}_{1-\alpha}(\mathbf{x}_{\text{test}}; \hat{\tau})$ achieves a finite-sample coverage guarantee, as Eq. 1 with the assumption of exchangeability (Lei et al., 2018). Despite the guarantee in expectation, the stability of coverage in different runs relies on the size of the calibration set. In particular, a small calibration set results in unnecessarily conservative prediction sets with high variability, which leads to divergent outcomes across different runs (Linusson et al., 2014; Vovk, 2013; Foygel Barber et al., 2021; Lei and Wasserman, 2014). In Appendix B, we present a mathematical analysis to show the relationship between the coverage variance and the size of calibration sets.

The issue of limited calibration sets To illustrate this, we empirically analyze how the calibration set size influences the coverage in split conformal prediction. We conduct experiments with varying numbers of labeled examples in calibration sets on ImageNet (Deng et al., 2009) with $\alpha = 0.1$. Figure 1a illustrates that with small calibration sets, empirical marginal coverage exhibits significant variability, frequently exceeding the target coverage of $1 - \alpha$. We further quantify this variability as the *Coverage Gap*, defined as $\Delta = \frac{1}{m} \sum_{i=1}^m |c_i - (1 - \alpha)|$, where c_i represents the empirical marginal coverage of the i -th run and m is the total number of runs. A larger coverage gap corresponds to a larger deviation of marginal coverage in multiple runs. Figures 1b and 1c demonstrate that small calibration sets result in both large coverage gaps and inflated prediction sets. With only 10 labeled data points, the average prediction set size increases by nearly 80% compared to using 500 examples. The results suggest that limited data in calibration sets causes inconsistent conformal prediction performance across different runs, reducing reliability and interpretability.

In the above analysis, we show that limited labeled data in calibration sets leads to both coverage variability and inflated prediction sets. To address this issue, previous works attempt to interpolate calibration instances or use modified p-value definitions, but they are heuristic and fail to provide finite-sample guarantees (Johansson et al., 2015; Carlsson et al., 2015). Besides, few-shot CP (Fisch et al., 2021) employs a meta-learning approach using similar auxiliary tasks, but its dependence on additional task collections limits practicality. This motivates us to explore another alternative - leveraging unlabelled data to address the data-scarce problem in the labeled calibration set.

To address this issue, previous works attempt to interpolate calibration instances or use modified p-value definitions, but they are heuristic and fail to provide finite-sample guarantees (Johansson et al., 2015; Carlsson et al., 2015). Besides, few-shot CP (Fisch et al., 2021) employs a meta-learning approach using similar auxiliary tasks, but its dependence on labeled data collections limits practicality. This motivates us to explore another alternative - leveraging unlabelled data to address the data-scarce problem in the labeled calibration set.

3 Method

In this work, we propose *SemiCP*, a semi-supervised framework of conformal prediction that leverages both labeled data and unlabeled data. In Subsection 3.1, we formalize *SemiCP* and identify the

necessary conditions for the coverage guarantee. Then, in Subsection 3.2, we introduce *NNM* – a novel method for generating nonconformity scores for unlabeled data that converge to the score distribution of unknown ground-truth labels.

3.1 Semi-supervised conformal prediction

In the semi-supervised setting, we consider a calibration dataset comprising both labeled and unlabeled examples: $\mathcal{D}^{\text{labeled}} = \{(\mathbf{x}_i, y_i)\}_{i=1}^n$ and $\mathcal{D}^{\text{unlabeled}} = \{(\tilde{\mathbf{x}}_i)\}_{i=1}^N$, which are i.i.d. sampled from $\mathcal{P}_{\mathcal{X}\mathcal{Y}}$. We denote by \tilde{y}_i the unknown true label of the unlabeled instance $\tilde{\mathbf{x}}_i$. In SemiCP, we compute nonconformity scores for both labeled and unlabeled examples in the calibration set. For each labeled example $(\mathbf{x}_i, y_i) \in \mathcal{D}^{\text{labeled}}$, we use commonly used nonconformity score functions $S(\cdot)$, e.g. THR (Sadinle et al., 2019), APS (Romano et al., 2020) or RAPS (Angelopoulos et al., 2020). For each unlabeled instance, we compute its nonconformity score $\tilde{s}_i = \tilde{S}(\tilde{\mathbf{x}}_i)$, $i = 1, \dots, N$ with a specially-designed unlabeled score function $\tilde{S}(\cdot)$ that does not require ground-truth labels. We will introduce our design of the unlabeled score function in Subsection 3.2.

Then, similar to Equation (2) in split conformal prediction, we aggregate the nonconformity scores of both labeled and unlabeled examples to estimate the threshold $\hat{\tau}_{\text{SemiCP}}$:

$$\hat{\tau}_{\text{SemiCP}} = \text{Quantile} \left(\{\tilde{s}_i\}_{i=1}^N \cup \{s_i\}_{i=1}^n, \frac{[(n + N + 1)(1 - \alpha)]}{n + N} \right). \quad (3)$$

With a proper unlabeled score function $\tilde{S}(\cdot)$, our SemiCP framework can enlarge the set of nonconformity scores from the calibration set with unlabeled examples, improving the accuracy and stability of threshold estimation. Given the estimated threshold $\hat{\tau}_{\text{SemiCP}}$, the prediction set for a test input \mathbf{x}_{test} is defined as: $\mathcal{C}_{\text{SemiCP}}(\mathbf{x}_{\text{test}}; \hat{\tau}_{\text{SemiCP}}) = \{y \in \mathcal{Y} : S(\mathbf{x}_{\text{test}}, y) \leq \hat{\tau}_{\text{SemiCP}}\}$. Now, we provide a formal requirement for the unlabeled score function to achieve valid coverage in SemiCP. Here we let \tilde{F}_s and F_s denote the cumulative distribution functions of the estimated and true nonconformity scores as $\tilde{F}_s(t) = \Pr(\tilde{S}(\tilde{\mathbf{x}}) \leq t)$, $F_s(t) = \Pr(S(\tilde{\mathbf{x}}, \tilde{y}) \leq t)$ for all $t \in \mathbb{R}$.

Proposition 1. *Let the labeled data $\{(\mathbf{x}_i, y_i)\}_{i=1}^n$ and the unlabeled data $\{\tilde{\mathbf{x}}_i\}_{i=1}^N$ be i.i.d. samples from the same underlying distribution. Suppose the estimated nonconformity scores $\tilde{S}(\tilde{\mathbf{x}}_i)$ share the same CDF as the true scores $S(\tilde{\mathbf{x}}, \tilde{y})$, i.e.*

$$\tilde{F}_s(t) = F_s(t), \quad \forall t \in \mathbb{R}.$$

Then the SemiCP prediction set satisfies the marginal coverage guarantee

$$\Pr(y_{\text{test}} \in \mathcal{C}_{\text{SemiCP}}(\mathbf{x}_{\text{test}})) \geq 1 - \alpha.$$

We present the proof in Appendix A.2. In other words, if the distribution of the approximated nonconformity scores for the unlabeled data is aligned with the distribution of the (unobserved) true scores, the estimated threshold $\hat{\tau}_{\text{SemiCP}}$ will coincide with the oracle threshold computed using fully labeled data, thus ensuring valid coverage as in standard conformal prediction. In order to meet the assumption of Prop. 1, we need to design $\tilde{S}(\tilde{\mathbf{x}})$ so that its distribution is consistent with that of the true score. In what follows, we introduce the unlabeled nonconformity score to satisfy this condition.

3.2 Nonconformity score for unlabeled data

Estimating nonconformity scores for unlabeled data is challenging because these scores depend on the unknown true labels. In other words, it is impractical to compute the exact scores of calibration data without the ground-truth. Instead, our key idea is to approximate the distribution of nonconformity scores, which is sufficient for valid SemiCP in Proposition 1. In what follows, we introduce our estimator that converges to the true scores in distribution.

Let f be a pre-trained model and $f_j(\tilde{\mathbf{x}}_i)$ be the softmax probability of class j for an unlabeled instance $\tilde{\mathbf{x}}_i$, then the pseudo label is $\hat{y}_i = \arg \max_{j \in \mathcal{Y}} f_j(\tilde{\mathbf{x}}_i)$. To obtain unlabeled non-conformity scores, a natural approach is to use pseudo labels \hat{y}_i to compute non-conformity scores with an existing scoring function $S(\cdot)$, e.g., THR and APS. We refer to the resulting values as *pseudo scores*: $\tilde{S}_{\text{naive}}(\tilde{\mathbf{x}}_i, S, f) = S(\tilde{\mathbf{x}}_i, \hat{y}_i)$. However, this estimator is systematically biased as the pseudo labels \hat{y}_i are always assigned the highest confidence, leading to low nonconformity scores. In other words, using the pseudo label leads to an underestimation of the true nonconformity score

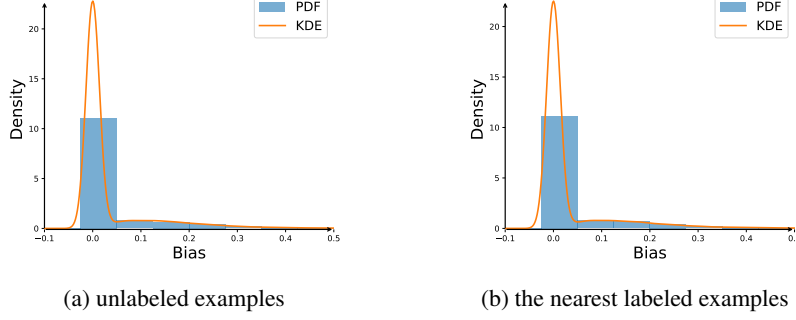


Figure 2: Distribution of pseudo bias for (a) unlabeled examples \tilde{x}_i and (b) the nearest labeled examples x_j that have the nearest *pseudo score* to the unlabeled examples

$S(\tilde{x}_i, \hat{y}_i) \leq S(\tilde{x}_i, \tilde{y}_i)$. To quantify the gap between pseudo scores and true scores, we define the *pseudo bias* as:

$$\Delta(\tilde{x}_i) := S(\tilde{x}_i, \tilde{y}_i) - S(\tilde{x}_i, \hat{y}_i).$$

In this work, we propose an unlabeled nonconformity score – **Nearest Neighbor Matching (NNM)**, which is rectified from the pseudo score with the nearest neighbor from the labeled set. In particular, we calculate *pseudo scores* for all labeled and unlabeled data in the calibration set. Then, for each unlabeled data \tilde{x}_i , we match a labeled data x_j that has the nearest *pseudo score* to the unlabeled data:

$$j = \arg \min_{j \in \{1, \dots, n\}} |S(\tilde{x}_i, \hat{y}_i) - S(x_j, \hat{y}_j)|.$$

In Figure 2, we demonstrate empirically that the pseudo bias distribution of the nearest labeled examples closely matches that of unlabeled examples. Thus, our key idea behind NNM is to approximate the pseudo bias $\Delta(\tilde{x})$ of unlabeled data with that of the nearest labeled example: $\Delta(\tilde{x}) \approx \Delta(x_j) = S(x_j, y_j) - S(x_j, \hat{y}_j)$, where x_j is the nearest labeled example of \tilde{x}_i .

With the approximated bias, we obtain the NNM score of an unlabeled example \tilde{x}_i by debiasing its pseudo score $S(\tilde{x}_i, \hat{y}_i)$:

$$\tilde{S}_{\text{nnm}}(\tilde{x}_i, D_{\text{labeled}}, S, f) = S(\tilde{x}_i, \hat{y}_i) + \Delta(x_j) = S(\tilde{x}_i, \hat{y}_i) + S(x_j, y_j) - S(x_j, \hat{y}_j), \quad (4)$$

where $S(\cdot)$ can be any existing score function, e.g., THR. In the following, we provide a theoretical analysis of the proposed unlabeled score function. Under mild continuity conditions, as the number of labeled examples n increases, our estimate \tilde{S}_{nnm} converges in distribution to the true nonconformity score $S(\tilde{x}_i, \tilde{y}_i)$. We present the Proof of Prop. 2 in Appendix 2.

Proposition 2. *Under Assumptions 1–4, let n be the number of labeled examples, and let $\tilde{F}_{\text{nnm}}(t)$ and $F_s(t)$ denote the cumulative distribution functions of \tilde{S}_{nnm} and S , respectively. Then, as $n \rightarrow \infty$, the NNM score function defined in Eq. (4) satisfies*

$$\tilde{F}_{\text{nnm}}(t) \rightarrow F_s(t) \quad \forall t \in \mathbb{R}.$$

The above theorem indicates that we can use the NNM score to approximate the true distribution of nonconformity scores, which is not directly available. Based on this, we can compute an approximate threshold $\hat{\tau}_{\text{SemiCP}}$ using Eq. (3). Since the calibration set incorporates a large number of unlabeled data points in addition to labeled data, $\hat{\tau}_{\text{SemiCP}}$ exhibits lower variance compared to the standard split CP threshold $\hat{\tau}$, resulting in a more stable estimate. Consequently, the corresponding conformal prediction sets are thus asymptotically valid as shown in Proposition 1. It is worth noting that the NNM score function is complementary to existing score functions (e.g., THR, APS, and RAPS), enhancing their stability and efficiency under limited calibration data.

SemiCP extends naturally to conditional conformal prediction by first partitioning both labeled and unlabeled calibration data into predefined groups (e.g., via feature-space clustering), then performing semi-supervised quantile estimation within each group to obtain group-specific thresholds $\hat{\tau}_{\text{SemiCP}}^g$. Applying these thresholds to test samples yields conditional coverage guarantees while still benefiting from reduced variance via unlabeled data. We provide the full algorithm for SemiCP and SemiCP-conditional in Appendix F, and we also provide a detailed analysis of NNM in Appendix C.

4 Experiments

4.1 Experimental setup

Datasets We evaluate our approach using three benchmarks of image classification: CIFAR-10, CIFAR-100 (Krizhevsky and Hinton, 2009), and ImageNet (Deng et al., 2009). Unless otherwise stated, for CIFAR-10 and CIFAR-100, we split the total of 10,000 samples into 4,000 for the labeled set, 4,000 for the unlabeled set, and 2,000 for the test set. For ImageNet, we partition 50,000 samples into 20,000 for the labeled set, 20,000 for the unlabeled set, and 10,000 for the test set. We additionally assess robustness under distribution shift and defer these results to Appendix H.4.

Models For most of our experiments, we used ResNet50 (He et al., 2016). In testing the generality of our approach across different models, we evaluate 10 different architectures, including ResNet (He et al., 2016), Mobilenet (Howard et al., 2019), ConvNet (Liu et al., 2022), EfficientNet (Tan and Le, 2021), ResNeXt (Xie et al., 2017), WideResNet (Zagoruyko and Komodakis, 2016), ViT (Dosovitskiy et al., 2020), MNASNet (Tan et al., 2019), and RegNet (Radosavovic et al., 2020). For ImageNet, we leverage pre-trained classifiers from TorchVision (maintainers and contributors, 2016), whereas for CIFAR-10 and CIFAR-100, we retrain the classifiers using the entire training set.

CP baselines We consider three score functions: THR, APS, and RAPS. For RAPS, we set $k_{\text{reg}} = 2$ and $\lambda = 0.01$. All experimental results are reported as the average performance across these three score functions, and the separate results of different score functions will be presented in detail in Appendix H.2. We use no random version of APS and RAPS, as the randomization of scores can impact the accuracy of the prediction scores. We will defer the adjustment for random factors to Appendix E and the results to Appendix H.8.

We present three methods in total: Standard, SemiCP, and Oracle. In the marginal coverage setting, **Standard** denotes the baseline Split CP applied to the dataset as a whole, which uses n labeled data points. In the group-conditional (Vovk et al., 2005) and class-conditional (Shi et al., 2013) settings, Standard applies CP independently to each group or class. In the group-conditional setting, we perform k-means clustering on the features of the calibration set images and divide them into 20 clusters. **SemiCP** refers to our proposed method, utilizes the same n labeled data points as Standard and additionally N unlabeled data points. **Oracle** represents the upper bound of CP performance by assuming access to labels of unlabeled data and running Split CP on a total of $n + N$ labeled data points. All of our experiments were repeated 1,000 trials.

Evaluation metrics The primary metrics for evaluating prediction sets are: (1) *CovGap* (Average Coverage Gap), which measures the average deviation from the target coverage across runs, and (2) *AvgSize* (Average Set Size), which reflects the efficiency of the prediction set. Smaller values for both metrics are desirable, though a smaller *AvgSize* is meaningful only if *CovGap* is small enough. This is because *AvgSize* may be artificially reduced due to undercoverage, resulting in an insufficient prediction set. The "improvement" refers to the enhancement of SemiCP relative to Oracle. We further provide a detailed result of over-coverage and under-coverage metrics in Appendix H.1. Detailed explanations of these metrics in different settings are provided in Appendix G.

4.2 Results

SemiCP enhances stability and efficiency of conformal prediction. Figure 3 compares the coverage gap and average set size of our proposed SemiCP method to that of Standard across varying amounts of labeled data, and results are averaged across three score functions. The results show that SemiCP consistently achieves smaller coverage gaps and compact prediction sets. For example, on CIFAR-10 with 10 labeled samples, SemiCP reduces the average coverage gap from 6.4 to 1.1 and decreases the average set size from 1.6 to 1.27. Moreover, as the number of labeled samples increases, SemiCP’s performance steadily improves, and its efficiency gradually approaches that of the oracle. These findings indicate that our method can reliably attain $1 - \alpha$ coverage while producing more efficient prediction sets.

SemiCP is consistently effective with varying amounts of unlabeled data. Figure 4 shows how the average coverage gap and prediction set size of SemiCP evolve as more unlabeled data are

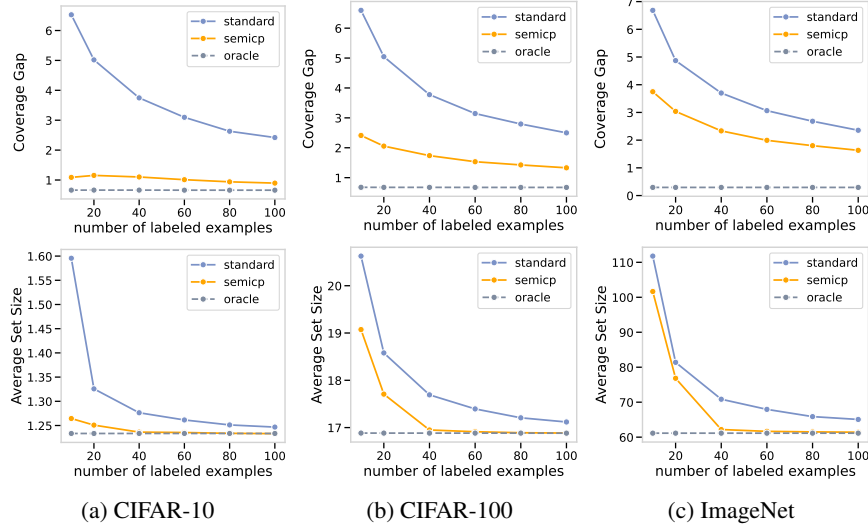


Figure 3: Average performance comparison of SemiCP with varying numbers of labeled data across three score functions on CIFAR-10, CIFAR-100, and ImageNet. The results demonstrate that SemiCP can enhance the stability and efficiency of existing score functions.

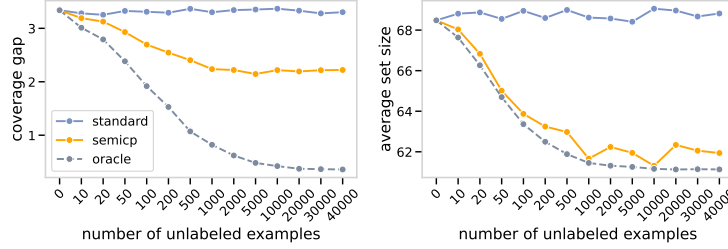


Figure 4: Average performance comparison of SemiCP with different numbers of unlabeled data across three score functions on ImageNet.

incorporated. We find that increasing the amount of unlabeled data steadily shrinks the coverage gap, bringing SemiCP’s performance closer to the Oracle and underscoring the value of unlabeled samples. At the same time, the average set size decreases markedly, demonstrating that SemiCP not only improves coverage but also yields more concise prediction sets. Notably, our method remains effective even with very few unlabeled examples. For instance, when $n = 50$ and $N = 10$, SemiCP still reduces the coverage gap by approximately 0.1 and the average set size by about 0.2, highlighting its robustness and broad applicability.

SemiCP generalizes effectively to conditional conformal prediction. Figure 5 reports the coverage gap and average set size of SemiCP when generalized to conditional conformal prediction on CIFAR100. Here, the horizontal axis n_{avg} denotes the average number of labeled examples per group or class. In the settings of class conditions and group conditions, SemiCP consistently outperforms the standard conformal method and even improves more than in the marginal coverage guarantee setting. For example, under class-conditional with $n_{\text{avg}} = 10$, SemiCP reduces the coverage gap from 7.75 to 6.29 and shrinks the average set size from 18.9 down to 17, drawing remarkably close to the oracle’s performance. These results demonstrate that SemiCP is not only effective in marginal coverage guarantees but also provides better stability and efficiency in conditional coverage guarantees.

SemiCP can benefit interpolation and ClusterCP. Some methods have been proposed to address its inherent trade-offs between stability and efficiency—examples include Interpolation, which refines the coverage threshold via linear interpolation around the $(1 - \alpha)$ -quantile when calibration data are scarce (Johansson et al., 2015), and ClusterCP, which groups classes by similar score distributions to compute group-specific thresholds for improved conditional coverage (Ding et al., 2024). Our SemiCP framework can be seamlessly integrated with these two methods, using NNM to calculate the

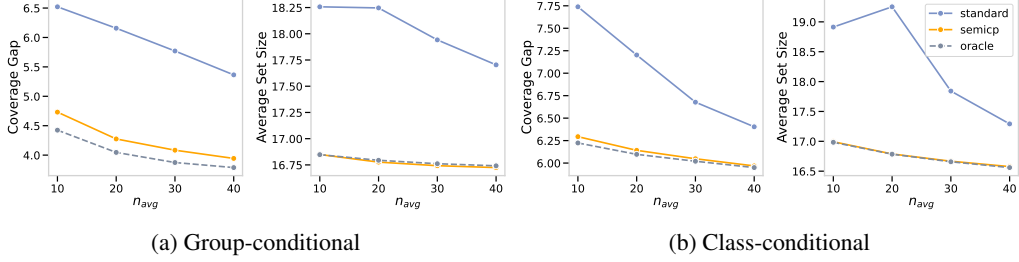


Figure 5: Average performance of SemiCP on CIFAR-100 under two conditional settings, including (a) group-condition and (b) class-condition. Results are averaged over three score functions.

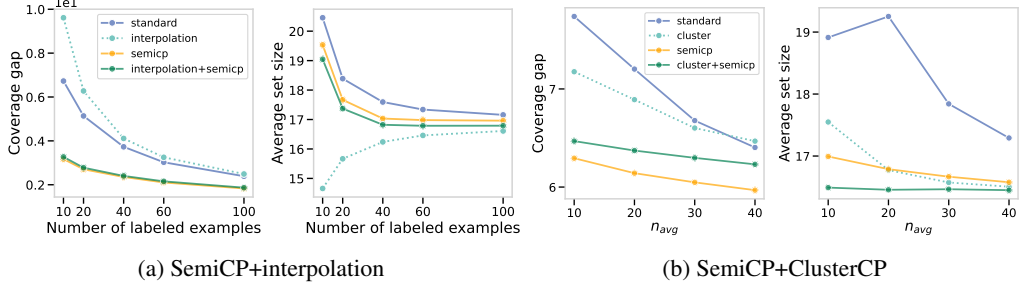


Figure 6: Average performance for the integration of SemiCP and (a) Interpolation and (b) ClusterCP, conducted on CIFAR100 using ResNet50 with three score functions.

unlabeled scores and incorporate them into the calibration set, and using these methods to calculate the threshold, further enhancing the reliability and efficiency of the prediction set.

Figure 6 demonstrates the efficacy of these integrations. While Interpolation alone generates a smaller prediction set, it suffers from a larger coverage gap compared to Standard, indicating greater instability and the inability to provide effective coverage guarantees. In contrast, integrating SemiCP with Interpolation reduces the coverage gap and average set size, achieving a decrease from 9 to 3.9 in the coverage gap when $n = 10$ and approaching the oracle’s set size for $n > 40$. Similarly, while ClusterCP alone improves both coverage and efficiency relative to Standard under low calibration budgets, the addition of SemiCP leads to further reductions in both average set size and coverage gap across all values of n_{avg} . These results confirm that SemiCP can be seamlessly integrated with existing methods to exploit unlabeled data and deliver more reliable, efficient predictive sets.

SemiCP works well with different model architectures. Figure 7 compares the performance of SemiCP on ten diverse ImageNet architectures. Across all these models, SemiCP reduces the mean coverage gap from 3.3 to 2.1, while simultaneously tightening the average prediction set size from 75 to 70.3, consistently outperforming the Standard method. These results highlight the model-agnostic nature of SemiCP and its ability to deliver consistent improvements in both coverage and efficiency across a wide range of architectures. Additionally, we provide an analysis of the impact of SemiCP on pseudo-label accuracy (i.e., model accuracy) in Appendix H.3.

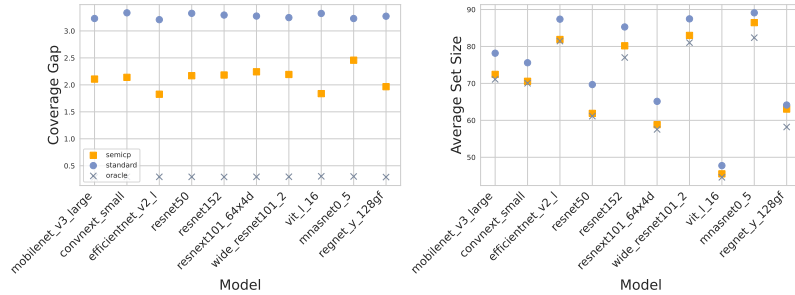


Figure 7: Average Coverage Gap and Set Size of SemiCP with different model architectures on ImageNet. The number of labeled data and unlabeled data is fixed at 50 and 20000.

5 Related work

Conformal prediction. Conformal Prediction (Vovk et al., 2005; Lei et al., 2018; Papadopoulos et al., 2002) provides a model-agnostic, finite-sample, and distribution-free framework for constructing prediction sets with coverage guarantees, and has been applied across various domains such as classification, regression (Romano et al., 2019; Xi et al., 2025), and large language models (Su et al., 2024; Cherian et al., 2024). In this work, we focus on the Split Conformal Prediction framework (Angelopoulos and Bates, 2021), where the training and calibration sets are separate. A key direction of research is conditional coverage, which involves obtaining coverage guarantees under specific conditions, such as when $X = x$ (X -conditional, usually relaxed to group-conditional) (Vovk et al., 2005; Gibbs et al., 2025) or $Y = y$ (Y -conditional, or class-conditional) (Shi et al., 2013; Löfström et al., 2015), enabling more contextually relevant prediction sets. Another important direction is the design of nonconformity scores, such as THR (Sadinle et al., 2019), APS (Romano et al., 2020), RAPS (Angelopoulos et al., 2020), and SAPS (Huang et al., 2023), which aim to improve the efficiency of prediction sets. However, current uncertainty scores generally rely on the ground-truth labels in calibration datasets. Our work is complementary to these labeled nonconformity scores and can be generalized to conditional coverage settings.

In the context of Conformal Prediction, the challenge of sample size has been discussed. Previous works (Linusson et al., 2014) analyzed the impact of calibration set size on CP performance and recommended using at least several hundred examples for calibration. This remains difficult to achieve, particularly in conditional coverage settings. For instance, in the case of Imagenet with 1,000 classes, if each class requires 100 calibration samples, a total of 100,000 calibration samples would be needed, which is impractical. To address this, prior efforts (Johansson et al., 2015) employ interpolation among the calibration instances, and Cluster-CP (Ding et al., 2024) groups data with similar conformal scores to ease sample-size requirements in class-conditional settings. Additionally, few-shot CP (Fisch et al., 2021) performs meta-learning in few-shot conformal prediction, leveraging labeled data from different tasks. However, none of these methods explore the use of unlabeled data to benefit conformal prediction. Our method not only overcomes these sample-size barriers, but also integrates seamlessly with these strategies to further improve coverage reliability and efficiency.

The benefits of unlabeled data. Beyond Conformal Prediction, semi-supervised learning has long been a popular direction, since unlabeled data is more cost-effective and accessible. Our work is closely related to research in semi-supervised inference, where unlabeled data is employed to enhance the performance of quantile estimation (Angelopoulos et al., 2023a,b; Zrnic and Candès, 2024; Cortes et al., 2008; Chakraborty et al., 2022b; Kim et al., 2024). Specifically, Prediction-powered inference (PPI) (Angelopoulos et al., 2023a) showed that leveraging accurate model predictions can further sharpen confidence intervals, a strategy subsequently applied in risk control (Einbinder et al., 2024), causal inference (Gao et al., 2024), distribution learning (Wen et al., 2024), and beyond. In this paper, we present the first method to leverage unlabeled data to improve the stability and efficiency of conformal prediction. A more detailed comparison between SemiCP and Semi-supervised quantile estimation can be found in Appendix D.

6 Conclusion

In this work, we introduced a novel framework, SemiCP, which leverages unlabeled data to achieve more stable and efficient prediction sets. Specifically, we approximate the true score distribution of unlabeled data through the proposed unlabeled score – Nearest Neighbor Matching (NNM). Extensive experimental results demonstrate that our approach consistently achieves coverage closer to the target and produces smaller prediction sets. Our method is simple, versatile, and straightforward to implement with conditional settings and different methods for improving conformal prediction. We hope that this framework will inspire future research to further explore the role of unlabeled data in conformal prediction.

Limitations. In this work, our theoretical results rely on the i.i.d. assumption for both labeled and unlabeled data, which is more strict than the exchangeability assumption in conformal prediction. It might be an interesting direction to explore semi-supervised conformal prediction under the exchangeability assumption.

References

- Anastasios N Angelopoulos and Stephen Bates. A gentle introduction to conformal prediction and distribution-free uncertainty quantification. *arXiv preprint arXiv:2107.07511*, 2021.
- Anastasios N Angelopoulos, Stephen Bates, Clara Fannjiang, Michael I Jordan, and Tijana Zrnic. Prediction-powered inference. *Science*, 382(6671):669–674, 2023a.
- Anastasios N Angelopoulos, John C Duchi, and Tijana Zrnic. Ppi++: Efficient prediction-powered inference. *arXiv preprint arXiv:2311.01453*, 2023b.
- Anastasios Nikolas Angelopoulos, Stephen Bates, Michael Jordan, and Jitendra Malik. Uncertainty sets for image classifiers using conformal prediction. In *International Conference on Learning Representations*, 2020.
- David Berthelot, Nicholas Carlini, Ian Goodfellow, Avital Oliver, Nicolas Papernot, and Colin Raffel. Mixmatch: a holistic approach to semi-supervised learning. *Advances in Neural Information Processing Systems*, 2019.
- Lars Carlsson, Ernst Ahlberg, Henrik Boström, Ulf Johansson, and Henrik Linusson. Modifications to p-values of conformal predictors. In *International Symposium on Statistical Learning and Data Sciences*, pages 251–259. Springer, 2015.
- Abhishek Chakraborty, Guorong Dai, and Raymond J Carroll. Semi-supervised quantile estimation: Robust and efficient inference in high dimensional settings. *arXiv preprint arXiv:2201.10208*, 2022a.
- Abhishek Chakraborty, Guorong Dai, and Raymond J Carroll. Semi-supervised quantile estimation: Robust and efficient inference in high dimensional settings. *arXiv preprint arXiv:2201.10208*, 2022b.
- John Cherian, Isaac Gibbs, and Emmanuel Candes. Large language model validity via enhanced conformal prediction methods. *Advances in Neural Information Processing Systems*, 37:114812–114842, 2024.
- Corinna Cortes, Mehryar Mohri, Michael Riley, and Afshin Rostamizadeh. Sample selection bias correction theory. In *Algorithmic Learning Theory*, page 38. Springer, 2008.
- Jesse C Cresswell, Yi Sui, Bhargava Kumar, and Noël Vouitsis. Conformal prediction sets improve human decision making. In *International Conference on Machine Learning*, 2024.
- Jia Deng, Wei Dong, Richard Socher, Li-Jia Li, Kai Li, and Li Fei-Fei. Imagenet: A large-scale hierarchical image database. In *2009 IEEE Conference on Computer Vision and Pattern Recognition*, pages 248–255. IEEE, 2009.
- Tiffany Ding, Anastasios Angelopoulos, Stephen Bates, Michael Jordan, and Ryan J Tibshirani. Class-conditional conformal prediction with many classes. *Advances in Neural Information Processing Systems*, 36, 2024.
- Alexey Dosovitskiy, Lucas Beyer, Alexander Kolesnikov, Dirk Weissenborn, Xiaohua Zhai, Thomas Unterthiner, Mostafa Dehghani, Matthias Minderer, Georg Heigold, Sylvain Gelly, et al. An image is worth 16x16 words: Transformers for image recognition at scale. In *International Conference on Learning Representations*, 2020.
- Bat-Sheva Einbinder, Liran Ringel, and Yaniv Romano. Semi-supervised risk control via prediction-powered inference. *arXiv preprint arXiv:2412.11174*, 2024.
- Adam Fisch, Tal Schuster, Tommi Jaakkola, and Regina Barzilay. Few-shot conformal prediction with auxiliary tasks. In *International Conference on Machine Learning*, 2021.
- Rina Foygel Barber, Emmanuel J Candes, Aaditya Ramdas, and Ryan J Tibshirani. The limits of distribution-free conditional predictive inference. *Information and Inference: A Journal of the IMA*, 10(2):455–482, 2021.

- Chenyin Gao, Peter B Gilbert, and Larry Han. On the role of surrogates in conformal inference of individual causal effects. *arXiv preprint arXiv:2412.12365*, 2024.
- Shanghua Gao, Zhong-Yu Li, Ming-Hsuan Yang, Ming-Ming Cheng, Junwei Han, and Philip Torr. Large-scale unsupervised semantic segmentation. *TPAMI*, 2022.
- Isaac Gibbs, John J Cherian, and Emmanuel J Candès. Conformal prediction with conditional guarantees. *Journal of the Royal Statistical Society Series B: Statistical Methodology*, 2025.
- Kaiming He, Xiangyu Zhang, Shaoqing Ren, and Jian Sun. Deep residual learning for image recognition. In *Proceedings of the IEEE Conference on Computer Vision and Pattern Recognition*, pages 770–778, 2016.
- Andrew Howard, Mark Sandler, Bo Chen, Weijun Wang, Liang-Chieh Chen, Mingxing Tan, Grace Chu, Vijay Vasudevan, Yukun Zhu, Ruoming Pang, et al. Searching for mobilenetv3. In *2019 IEEE/CVF International Conference on Computer Vision*, pages 1314–1324. IEEE, 2019.
- Gao Huang, Zhuang Liu, Laurens Van Der Maaten, and Kilian Q Weinberger. Densely connected convolutional networks. In *2017 IEEE Conference on Computer Vision and Pattern Recognition*, pages 2261–2269. IEEE, 2017.
- Jianguo Huang, HuaJun Xi, Linjun Zhang, Huaxiu Yao, Yue Qiu, and Hongxin Wei. Conformal prediction for deep classifier via label ranking. In *International Conference on Machine Learning*, 2023.
- Jianguo Huang, Jianqing Song, Xuanning Zhou, Bingyi Jing, and Hongxin Wei. Torchcp: A python library for conformal prediction. *arXiv preprint arXiv:2402.12683*, 2024.
- Ulf Johansson, Ernst Ahlberg, Henrik Boström, Lars Carlsson, Henrik Linusson, and Cecilia Sönströd. Handling small calibration sets in mondrian inductive conformal regressors. In *International Symposium on Statistical Learning and Data Sciences*, pages 271–280. Springer, 2015.
- Kevin Kasa, Zhiyu Zhang, Heng Yang, and Graham W Taylor. Adapting conformal prediction to distribution shifts without labels. *arXiv preprint arXiv:2406.01416*, 2024.
- Ilmun Kim, Larry Wasserman, Sivaraman Balakrishnan, and Matey Neykov. Semi-supervised u-statistics. *arXiv preprint arXiv:2402.18921*, 2024.
- Shayan Kiyani, George J Pappas, and Hamed Hassani. Conformal prediction with learned features. In *International Conference on Machine Learning*, 2024.
- Simon Kornblith, Jonathon Shlens, and Quoc V Le. Do better imagenet models transfer better? In *2019 IEEE/CVF Conference on Computer Vision and Pattern Recognition*, pages 2656–2666. IEEE, 2019.
- A. Krizhevsky and G. Hinton. Learning multiple layers of features from tiny images. *Master’s thesis, Department of Computer Science, University of Toronto*, 2009.
- Jing Lei and Larry Wasserman. Distribution-free prediction bands for non-parametric regression. *Journal of the Royal Statistical Society Series B: Statistical Methodology*, 76(1):71–96, 2014.
- Jing Lei, Max G’Sell, Alessandro Rinaldo, Ryan J Tibshirani, and Larry Wasserman. Distribution-free predictive inference for regression. *Journal of the American Statistical Association*, 113(523): 1094–1111, 2018.
- Henrik Linusson, Ulf Johansson, Henrik Boström, and Tuve Löfström. Efficiency comparison of unstable transductive and inductive conformal classifiers. In *10th IFIP International Conference on Artificial Intelligence Applications and Innovations (AIAI)*, pages 261–270. Springer, 2014.
- Zhuang Liu, Hanzi Mao, Chao-Yuan Wu, Christoph Feichtenhofer, Trevor Darrell, and Saining Xie. A convnet for the 2020s. In *2022 IEEE/CVF Conference on Computer Vision and Pattern Recognition*, pages 11966–11976. IEEE, 2022.
- Tuve Löfström, Henrik Boström, Henrik Linusson, and Ulf Johansson. Bias reduction through conditional conformal prediction. *Intelligent Data Analysis*, 19(6):1355–1375, 2015.

- TorchVision maintainers and contributors. Torchvision: Pytorch’s computer vision library. <https://github.com/pytorch/vision>, 2016.
- Roberto I Oliveira, Paulo Orenstein, Thiago Ramos, and João Vitor Romano. Split conformal prediction and non-exchangeable data. *Journal of Machine Learning Research*, 25(225):1–38, 2024.
- Henrik Olsson, Kimmo Kartasalo, Nita Mulliqi, Marco Capuccini, Pekka Ruusuvuori, Hemamali Samarutunga, Brett Delahunt, Cecilia Lindskog, Emiel AM Janssen, Anders Blilie, et al. Estimating diagnostic uncertainty in artificial intelligence assisted pathology using conformal prediction. *Nature Communications*, 13(1):7761, 2022.
- Harris Papadopoulos, Kostas Proedrou, Volodya Vovk, and Alex Gammerman. Inductive confidence machines for regression. In *Machine learning: ECML 2002: 13th European conference on machine learning Helsinki, Finland, August 19–23, 2002 proceedings 13*, pages 345–356. Springer, 2002.
- Ilija Radosavovic, Raj Prateek Kosaraju, Ross Girshick, Kaiming He, and Piotr Dollár. Designing network design spaces. In *2020 IEEE/CVF Conference on Computer Vision and Pattern Recognition*, pages 10425–10433. IEEE, 2020.
- Benjamin Recht, Rebecca Roelofs, Ludwig Schmidt, and Vaishaal Shankar. Do imagenet classifiers generalize to imagenet? In *NeurIPS 2021 Workshop on ImageNet: Past, Present, and Future*, 2019.
- Yaniv Romano, Evan Patterson, and Emmanuel Candes. Conformalized quantile regression. *Advances in Neural Information Processing Systems*, 32, 2019.
- Yaniv Romano, Matteo Sesia, and Emmanuel Candes. Classification with valid and adaptive coverage. *Advances in Neural Information Processing Systems*, 33:3581–3591, 2020.
- Mauricio Sadinle, Jing Lei, and Larry Wasserman. Least ambiguous set-valued classifiers with bounded error levels. *Journal of the American Statistical Association*, 114(525):223–234, 2019.
- Glenn Shafer and Vladimir Vovk. A tutorial on conformal prediction. *Journal of Machine Learning Research*, 9(3), 2008.
- Fan Shi, Cheng Soon Ong, and Christopher Leckie. Applications of class-conditional conformal predictor in multi-class classification. In *2013 12th International Conference on Machine Learning and Applications*, volume 1, pages 235–239. IEEE, 2013.
- Jianqing Song, Jianguo Huang, Wenyu Jiang, Baoming Zhang, Shuangjie Li, and Chongjun Wang. Similarity-navigated conformal prediction for graph neural networks. *Advances in Neural Information Processing Systems*, 2024.
- Jiayuan Su, Jing Luo, Hongwei Wang, and Lu Cheng. Api is enough: Conformal prediction for large language models without logit-access. In *Findings of the Association for Computational Linguistics: EMNLP 2024*, pages 979–995, 2024.
- Mingxing Tan and Quoc V Le. Efficientnetv2: Smaller models and faster training. In *International Conference on Machine Learning*, 2021.
- Mingxing Tan, Bo Chen, Ruoming Pang, Vijay Vasudevan, Mark Sandler, Andrew Howard, and Quoc V Le. Mnasnet: platform-aware neural architecture search for mobile. In *2019 IEEE/CVF Conference on Computer Vision and Pattern Recognition*, pages 2815–2823. IEEE, 2019.
- Jesper E Van Engelen and Holger H Hoos. A survey on semi-supervised learning. *Machine learning*, 109(2):373–440, 2020.
- Janette Vazquez and Julio C Facelli. Conformal prediction in clinical medical sciences. *Journal of Healthcare Informatics Research*, 6(3):241–252, 2022.
- Vladimir Vovk. Conditional validity of inductive conformal predictors. *Machine Learning*, 92(2-3): 349–376, 2013.

- Vladimir Vovk and Claus Bendtsen. Conformal predictive decision making. In *Conformal and Probabilistic Prediction and Applications*, pages 52–62. PMLR, 2018.
- Vladimir Vovk, David Lindsay, Ilia Nouretdinov, and Alex Gammerman. Mondrian confidence machine. *Technical Report*, 2003.
- Vladimir Vovk, Alexander Gammerman, and Glenn Shafer. *Algorithmic learning in a random world*, volume 29. Springer, 2005.
- Mengtao Wen, Yinxu Jia, Haojie Ren, Zhaojun Wang, and Changliang Zou. Semi-supervised distribution learning. *Biometrika*, 112(1):asae056, 10 2024.
- Huajun Xi, Kangdao Liu, Hao Zeng, Wenguang Sun, and Hongxin Wei. Robust online conformal prediction under uniform label noise. *arXiv preprint arXiv:2501.18363*, 2025.
- Saining Xie, Ross Girshick, Piotr Dollár, Zhuowen Tu, and Kaiming He. Aggregated residual transformations for deep neural networks. In *2017 IEEE Conference on Computer Vision and Pattern Recognition*, pages 5987–5995. IEEE, 2017.
- Wenxiang Xu. Strong baselines for cifar100. <https://github.com/tcmlyxc/Strong-Baselines-for-CIFAR100>, 2024.
- Sergey Zagoruyko and Nikos Komodakis. Wide residual networks. In *British Machine Vision Conference 2016*. British Machine Vision Association, 2016.
- Soroush H Zargarbashi, Simone Antonelli, and Aleksandar Bojchevski. Conformal prediction sets for graph neural networks. In *International Conference on Machine Learning*, 2023.
- Xiaohua Zhai, Avital Oliver, Alexander Kolesnikov, and Lucas Beyer. S4l: Self-supervised semi-supervised learning. In *2019 IEEE/CVF International Conference on Computer Vision*, pages 1476–1485. IEEE, 2019.
- Biao Zhang. Estimating a distribution function in the presence of auxiliary information. *Metrika*, 46(1):221–244, 1997.
- Tijana Zrnic and Emmanuel J Candès. Cross-prediction-powered inference. *Proceedings of the National Academy of Sciences*, 121(15):e2322083121, 2024.

A Proofs

A.1 Notation.

Table 1: Notations used in this paper.

Symbol	Description
$\mathcal{D}_{\text{labeled}} = \{(\mathbf{x}_j, y_j)\}_{j=1}^n$	Labeled dataset
$\mathcal{D}_{\text{unlabeled}} = \{\tilde{\mathbf{x}}_i\}_{i=1}^N$	Unlabeled dataset (with unknown labels \tilde{y}_i)
$S(\mathbf{x}, y)$	Nonconformity score function for labeled data
$\tilde{S}(\tilde{\mathbf{x}})/\hat{S}(\tilde{\mathbf{x}}, \mathcal{D}_{\text{labeled}}, S, f)$	Nonconformity score function for unlabeled data
\hat{y}	Model prediction for specific input $\mathbf{x}/\tilde{\mathbf{x}}$
$\hat{\tau}_{\text{SemiCP}}$	Quantile threshold computed by SemiCP
$\mathcal{C}_{\text{SemiCP}}(\mathbf{x})$	SemiCP prediction set: $\{y : S(\mathbf{x}, y) \leq \hat{\tau}_{\text{SemiCP}}\}$
$\hat{\tau}_{\text{Oracle}}$	Quantile threshold computed by standard method with labeled data and unlabeled data
$\mathcal{C}_{\text{Oracle}}(\mathbf{x})$	Oracle prediction set: $\{y : S(\mathbf{x}, y) \leq \hat{\tau}_{\text{Oracle}}\}$
$F_s(t)$	CDF of oracle scores: $\mathbb{P}(S(\mathbf{x}, y) \leq t)$
$\tilde{F}_s(t)$	CDF of estimated scores: $\mathbb{P}(\tilde{S}(\tilde{\mathbf{x}}) \leq t)$
$\tilde{U}_i = S(\tilde{\mathbf{x}}_i, \hat{y})$	Pseudo-score for unlabeled input
$\tilde{V}_i = S(\tilde{\mathbf{x}}_i, \tilde{y}_i)$	True score for unlabeled input
$U_j = S(\mathbf{x}_j, \hat{y})$	Pseudo-score for labeled input
$V_j = S(\mathbf{x}_j, y_j)$	True score for labeled input
$\Delta_j = V_j - U_j$	Observed bias from labeled point \mathbf{x}_j
$\Delta(\tilde{\mathbf{x}}_i) = \tilde{V}_i - \tilde{U}_i$	True bias at unlabeled point $\tilde{\mathbf{x}}_i$
$\mathcal{N}_n(\tilde{\mathbf{x}}_i, R_n)$	Radius- R_n neighborhood of $\tilde{\mathbf{x}}_i$

A.2 Proof of Proposition 1

Proof. Let $\hat{\tau}_{\text{Oracle}}$ denote the $(1 - \alpha)$ empirical quantile of the oracle nonconformity scores $\{S(\mathbf{x}_i, y_i)\}_{i=1}^n \cup \{S(\tilde{\mathbf{x}}_i, \tilde{y}_i)\}_{i=1}^N$, computed using both labeled and unlabeled data. Let $\hat{\tau}_{\text{SemiCP}}$ be the threshold defined as in Equation (3).

By assumption, the estimated and oracle nonconformity scores are identically distributed:

$$\tilde{F}_s(t) = F_s(t), \quad \forall t \in \mathbb{R},$$

which implies that their corresponding empirical quantiles are equal in distribution:

$$\hat{\tau}_{\text{SemiCP}} \stackrel{d}{=} \hat{\tau}_{\text{Oracle}}.$$

Moreover, the test score $S(\mathbf{x}_{\text{test}}, y_{\text{test}})$ is drawn from the same distribution as the calibration scores. Therefore,

$$\mathbb{P}(S(\mathbf{x}_{\text{test}}, y_{\text{test}}) \leq \hat{\tau}_{\text{SemiCP}}) = \mathbb{P}(S(\mathbf{x}_{\text{test}}, y_{\text{test}}) \leq \hat{\tau}_{\text{Oracle}}).$$

By the standard conformal prediction guarantee, the oracle prediction set satisfies:

$$\mathbb{P}(y_{\text{test}} \in \mathcal{C}_{\text{Oracle}}(\mathbf{x}_{\text{test}}, \hat{\tau}_{\text{Oracle}})) \geq 1 - \alpha.$$

Therefore, the same coverage guarantee holds for the SemiCP prediction set:

$$\mathbb{P}(y_{\text{test}} \in \mathcal{C}_{\text{SemiCP}}(\mathbf{x}_{\text{test}}, \hat{\tau}_{\text{SemiCP}})) \geq 1 - \alpha.$$

□

A.3 Proof of proposition 2.

Assumption 1. (i.i.d. Data) The labeled data $\{(\mathbf{x}_j, y_j)\}_{j=1}^n$ and unlabeled data points $\{\tilde{\mathbf{x}}_i\}_{i=1}^N$ (with their true labels \tilde{y}_i) are independent and identically distributed according to a joint distribution P_{XY} on $\mathcal{X} \times \mathcal{Y}$.

Assumption 2. (Continuity of Functions) The pseudo-label score function $u(\mathbf{x}) = S(\mathbf{x}, \hat{y})$ and the true score function $v(\mathbf{x}, y) = S(\mathbf{x}, y)$ are continuous functions (specifically, continuous in \mathbf{x} for fixed y if \mathcal{Y} is discrete).

Assumption 3. (Continuity of Random Variables) The random variables $U = u(\mathbf{x})$ and $V = v(\mathbf{x}, y)$ have continuous cumulative distribution functions (CDFs).

Assumption 4. (Restricted Search Conditions)

- (a) There exists a sequence of radii $\{R_n\}_{n=1}^\infty$ such that $R_n > 0$ for all n and $\lim_{n \rightarrow \infty} R_n = 0$.
- (b) The sequence $\{R_n\}$ converges to 0 sufficiently slowly such that for P_X -almost every $\tilde{\mathbf{x}} \in \mathcal{X}$ (in particular, for $\tilde{\mathbf{x}} = \tilde{\mathbf{x}}_i$, $i = 1, \dots, N$), the expected number of labeled points within distance R_n grows unboundedly, i.e.,

$$\lim_{n \rightarrow \infty} n \cdot P_X(B(\tilde{\mathbf{x}}, R_n)) = \infty$$

where $B(\tilde{\mathbf{x}}, R_n) = \{\mathbf{x} \in \mathcal{X} : \|\mathbf{x} - \tilde{\mathbf{x}}\| < R_n\}$.

- (c) The marginal distribution P_X has positive density in the neighborhood of each $\tilde{\mathbf{x}}_i$, $i = 1, \dots, N$.

Proof. For theoretical simplicity, we let the NNM score $\tilde{S}_{nnm}(\tilde{\mathbf{x}}_i)$ for unlabeled point $\tilde{\mathbf{x}}_i$ be computed using a modified matching rule: first restrict the search for neighbors j to the set $\mathcal{N}_n(\tilde{\mathbf{x}}_i, R_n) = \{j \in \{1, \dots, n\} : \|\mathbf{x}_j - \tilde{\mathbf{x}}_i\| < R_n\}$, and then find the nearest neighbor j^* : $j^* = \arg \min_{j \in \mathcal{N}_n} |U_j - \tilde{U}_i|$.

We aim to show $\tilde{F}_{nnm}(t) \xrightarrow{P} F_s(t)$ as $n \rightarrow \infty$ for fixed N . This follows if we show that for each $i \in \{1, \dots, N\}$, the NNM score $\tilde{S}_{nnm}(\tilde{\mathbf{x}}_i)$ converges in probability to the true score $\tilde{V}_i = S(\tilde{\mathbf{x}}_i, \tilde{y}_i)$. Let $V_j = v(\mathbf{x}_j, y_j)$ and $U_j = u(\mathbf{x}_j)$. Let $\tilde{V}_i = v(\tilde{\mathbf{x}}_i, \tilde{y}_i)$ and $\tilde{U}_i = u(\tilde{\mathbf{x}}_i)$. The modified matching rule selects j^* as:

1. Define $\mathcal{N}_n(\tilde{\mathbf{x}}_i, R_n) = \{j \in \{1, \dots, n\} : \|\mathbf{x}_j - \tilde{\mathbf{x}}_i\| < R_n\}$. By Assumption 4(b,c), $P(\mathcal{N}_n(\tilde{\mathbf{x}}_i, R_n) \neq \emptyset) \rightarrow 1$ as $n \rightarrow \infty$. We proceed conditionally on \mathcal{N}_n being non-empty.
2. $j^* = \arg \min_{j \in \mathcal{N}_n(\tilde{\mathbf{x}}_i, R_n)} |U_j - \tilde{U}_i|$.

The NNM score is $\tilde{S}_{nnm}(\tilde{\mathbf{x}}_i) = \tilde{U}_i + V_{j^*} - U_{j^*}$. We want to show $|\tilde{S}_{nnm}(\tilde{\mathbf{x}}_i) - \tilde{V}_i| \xrightarrow{P} 0$. Using the triangle inequality:

$$|\tilde{S}_{nnm}(\tilde{\mathbf{x}}_i) - \tilde{V}_i| = |(\tilde{U}_i - U_{j^*}) + (V_{j^*} - \tilde{V}_i)| \leq |\tilde{U}_i - U_{j^*}| + |V_{j^*} - \tilde{V}_i|$$

We show convergence in probability to 0 for both terms on the right-hand side.

Convergence of V_{j^*} : By definition of j^* , we have $j^* \in \mathcal{N}_n(\tilde{\mathbf{x}}_i, R_n)$, which implies $\|\mathbf{x}_{j^*} - \tilde{\mathbf{x}}_i\| < R_n$. By Assumption 4(a), $\lim_{n \rightarrow \infty} R_n = 0$. Therefore, for any $\delta > 0$,

$$P(\|\mathbf{x}_{j^*} - \tilde{\mathbf{x}}_i\| \geq \delta) \leq P(R_n \geq \delta) \rightarrow 0 \quad \text{as } n \rightarrow \infty$$

This establishes $\mathbf{x}_{j^*} \xrightarrow{P} \tilde{\mathbf{x}}_i$. Since $v(\mathbf{x}, y)$ is continuous in \mathbf{x} (Assumption 2), by the Continuous Mapping Theorem (CMT),

$$V_{j^*} = v(\mathbf{x}_{j^*}, y_{j^*}) \xrightarrow{P} v(\tilde{\mathbf{x}}_i, \tilde{y}_i) = \tilde{V}_i$$

Hence, $|V_{j^*} - \tilde{V}_i| \xrightarrow{P} 0$.

Convergence of U_{j^*} : Since $u(\mathbf{x})$ is continuous in \mathbf{x} (Assumption 2), and we have shown $\mathbf{x}_{j^*} \xrightarrow{P} \tilde{\mathbf{x}}_i$, by the CMT,

$$U_{j^*} = u(\mathbf{x}_{j^*}) \xrightarrow{P} u(\tilde{\mathbf{x}}_i) = \tilde{U}_i$$

Hence, $|\tilde{U}_i - U_{j^*}| \xrightarrow{P} 0$.

Conclusion for pointwise convergence: Since $|\tilde{U}_i - U_{j^*}| \xrightarrow{P} 0$ and $|V_{j^*} - \tilde{V}_i| \xrightarrow{P} 0$, their sum also converges to 0 in probability. By the Squeeze Theorem,

$$|\tilde{S}_{nnm}(\tilde{\mathbf{x}}_i) - \tilde{V}_i| \xrightarrow{P} 0.$$

□

B Theoretical analysis of conformal prediction with small calibration set

In Section 2, we showed empirically that when the calibration set is small, the observed marginal coverage can vary substantially, and the resulting prediction sets tend to be overly large. Here, we provide a theoretical explanation of this phenomenon.

When the calibration size n is small, the threshold $\hat{\tau}$ becomes highly variable, which in turn leads to fluctuations in the coverage probability on unseen test data (Linusson et al., 2014). Concretely, assuming the nonconformity scores are continuous, the coverage given the calibration set follows a Beta distribution (Vovk, 2013; Angelopoulos et al., 2023a; Ding et al., 2024):

$$\mathbb{P}(Y_{\text{test}} \in \mathcal{C}_{1-\alpha}(\mathbf{x}_{\text{test}}) \mid \mathcal{D}_{\text{cal}}) \sim \text{Beta}(l_{\alpha}^n, n+1-l_{\alpha}^n),$$

where $l_{\alpha}^n = \lceil (n+1)(1-\alpha) \rceil$. Its expectation is $\ell/(n+1) \approx 1-\alpha$, but its variance

$$\frac{l_{\alpha}^n(n+1-l_{\alpha}^n)}{(n+1)^2(n+2)} \approx \frac{\alpha(1-\alpha)}{n+2},$$

can be large when n is small. For instance, if $n = 10$ and $\alpha = 0.1$, then $\ell = 10$ and $\Pr(y_{\text{test}} \in \mathcal{C}_{0.9}(\mathbf{x}_{\text{test}}) \mid \mathcal{D}_{\text{cal}}) \sim \text{Beta}(10, 1)$, whose high variance yields overly conservative sets: the expected coverage overshoots $1-\alpha$ by about 0.066, yet there remains a 10.7% probability that coverage falls below 80%.

C Detailed analysis of unlabeled nonconformity score function

To understand the effectiveness of the Nearest Neighbor Matching (NNM) approach for estimating the nonconformity scores of unlabeled examples, we compare it against several baseline methods of increasing complexity:

1. **Naive:** Uses the nonconformity score of the pseudo-label as the prediction:

$$\tilde{S}_{\text{naive}}(\tilde{\mathbf{x}}_i, S, f) = S(\tilde{\mathbf{x}}_i, \hat{y}_i).$$

2. **Debias:** Applies a global correction by adding the average discrepancy between the true and pseudo nonconformity scores computed on labeled data:

$$\tilde{S}_{\text{debias}}(\tilde{\mathbf{x}}_i, D_{\text{labeled}}, S, f) = S(\tilde{\mathbf{x}}_i, \hat{y}_i) + \frac{1}{n} \sum_{j=1}^n [S(\mathbf{x}_j, y_j) - S(\mathbf{x}_j, \hat{y}_j)].$$

3. **Random Match (RM):** Adds a bias correction using a randomly selected labeled example from the dataset:

$$\tilde{S}_{\text{rm}}(\tilde{\mathbf{x}}_i; D_{\text{labeled}}, S, f) = S(\tilde{\mathbf{x}}_i, \hat{y}_i) + S(\mathbf{x}_j, y_j) - S(\mathbf{x}_j, \hat{y}_j), \quad j \sim \text{Uniform}\{1, \dots, n\}.$$

4. **Nearest Neighbor Matching (NNM):** Selects a labeled example whose pseudo nonconformity score is closest to that of the unlabeled input, and uses it to construct a local bias correction:

$$\begin{aligned} \tilde{S}_{\text{nnm}}(\tilde{\mathbf{x}}_i, D_{\text{labeled}}, S, f) &= S(\tilde{\mathbf{x}}_i, \hat{y}_i) + S(\mathbf{x}_j, y_j) - S(\mathbf{x}_j, \hat{y}_j), \\ \text{where } j &= \arg \min_{j \in \{1, \dots, n\}} |S(\tilde{\mathbf{x}}_i, \hat{y}_i) - S(\mathbf{x}_j, \hat{y}_j)|. \end{aligned}$$

Why naive estimation is biased. The naive method estimates the nonconformity score of an unlabeled input $\tilde{\mathbf{x}}_i$ by evaluating the score at the model’s predicted label \hat{y}_i , i.e., $\tilde{S}_{\text{naive}}(\tilde{\mathbf{x}}_i) = S(\tilde{\mathbf{x}}_i, \hat{y}_i)$. By definition, the pseudo-label \hat{y}_i corresponds to the most confident class under the model, and hence its nonconformity score is typically the smallest among all possible labels.

As a result, the naive method systematically underestimates the true nonconformity score, since \tilde{y}_i may not coincide with the model prediction. This underestimation leads to an underestimated quantile threshold and, consequently, a conformal prediction set that is too narrow. In turn, this violates the target coverage guarantee, as the predicted set is less likely to contain the true label.

Why the *Debias* method is inconsistent. The debias method attempts to correct the naive estimate by adding the global average bias observed on the labeled calibration set:

$$\tilde{S}_{\text{debias}}(\tilde{x}_i) = \tilde{U}_i + \bar{\Delta}_n, \quad \text{where} \quad \bar{\Delta}_n = \frac{1}{n} \sum_{j=1}^n (V_j - U_j).$$

By the law of large numbers, $\bar{\Delta}_n \xrightarrow{p} \mathbb{E}[\Delta(X)]$, the expected bias across the entire input space. However, this correction ignores the local context of \tilde{X}_i , and generally $\Delta(\tilde{X}_i) \neq \mathbb{E}[\Delta(X)]$, especially when the bias function $\Delta(X)$ varies spatially. As a result, $\tilde{S}_{\text{debias}}(\tilde{x}_i)$ converges to the wrong target and is therefore inconsistent for the true score \tilde{V}_i .

Why *random match* is suboptimal. The random match (RM) method improves upon debias by using a labeled instance j drawn uniformly from a local neighborhood $\mathcal{N}_n(\tilde{x}_i, R_n)$, and correcting the pseudo-score using its observed bias:

$$\tilde{S}_{\text{rm}}(\tilde{x}_i) = \tilde{U}_i + \Delta_j, \quad j \sim \text{Uniform}(\mathcal{N}_n).$$

This guarantees that $\|x_j - \tilde{x}_i\| \rightarrow 0$, helping control the error $|V_j - \tilde{V}_i|$. However, RM does not consider the pseudo-score \tilde{U}_i when selecting j , meaning the matched point may differ significantly in model confidence. This neglect can result in poor approximation of $\Delta(\tilde{x}_i)$, especially in regions where the model’s bias is heterogeneous, thereby limiting RM’s accuracy in finite samples.

Why *Nearest Neighbor Matching* is superior. Nearest Neighbor Matching (NNM) enhances RM by selecting, within the same neighborhood, the point j^* whose pseudo-score U_j is closest to \tilde{U}_i :

$$\tilde{S}_{\text{nnm}}(\tilde{x}_i) = \tilde{U}_i + \Delta_{j^*}, \quad j^* = \arg \min_{j \in \mathcal{N}_n} |U_j - \tilde{U}_i|.$$

This matching leverages both feature-space proximity and pseudo-score similarity, yielding a local and adaptive bias correction. Under mild continuity assumptions, we can show that $x_{j^*} \xrightarrow{p} \tilde{x}_i$, and thus $\Delta_{j^*} \xrightarrow{p} \Delta(\tilde{x}_i)$, making NNM an asymptotically consistent estimator. Moreover, NNM achieves lower estimation error in finite samples by selecting a neighbor that better matches both the location and the model output, making it theoretically sound and practically more effective.

Finally, we present the experimental results of coverage gap and prediction set size for these four methods in Appendix H.5, demonstrating that our approach achieves the best improvement in the stability and efficiency of CP. Additionally, we provide ablation studies on the selection criteria and number of nearest neighbors in Appendix H.6 and Appendix H.7, respectively.

D SemiCP vs. Semi-supervised Quantile Estimation

Our approach, SemiCP, addresses the inaccuracy of quantile estimation in conformal prediction (CP) by incorporating nonconformity scores computed for each unlabeled observation into the calibration process. In contrast, semi-supervised quantile estimation methods (Zhang, 1997; Chakraborty et al., 2022a; Angelopoulos et al., 2023a) leverage auxiliary unlabeled data directly to estimate quantiles. Below, we summarize the key innovations and advantages of SemiCP:

1. **Training-free and information-efficient.** Semi-supervised quantile estimation typically requires auxiliary information (Zhang, 1997), the training of additional models (Chakraborty et al., 2022a), or iterative optimization such as gradient descent (Angelopoulos et al., 2023a). In contrast, SemiCP requires no extra data beyond the standard CP inputs and is entirely training-free.
2. **Nonconformity-based per-point scores.** Traditional semi-supervised quantile estimation yields a single, global quantile estimate, whereas SemiCP computes a nonconformity score for each unlabeled instance, directly incorporating the core CP concept of nonconformity. This per-point scoring confers several benefits: it naturally extends to conditional conformal prediction, facilitates integration with other CP enhancements, and yields more fine-grained uncertainty measures. We demonstrate these advantages and report significant empirical gains in Section 4.2.

3. **Compatibility with randomized score functions.** Many CP score functions—such as APS (Romano et al., 2020), RAPS (Angelopoulos et al., 2020), and SAPS (Huang et al., 2023)—incorporate randomization that cannot be captured by parametric models. Semi-supervised quantile estimation fails to adapt to these randomized scores, whereas SemiCP can easily accommodate them. In Appendix E, we outline the adaptation strategy, and in Appendix H.8 we present corresponding experimental results.

E Unlabeled nonconformity score with random factor

In the main experiments, we employ the non-random version of the nonconformity score, as the introduction of a random factor can influence the nearest-neighbor matching process. However, some nonconformity scores, such as APS, utilize randomization techniques to get tighter prediction sets. In this section, we describe how to incorporate a random factor into the Nearest-Neighbor Matching (NNM) method.

Let the score with a random factor be denoted as $S(\mathbf{x}_i, y_i, u_i)$, where u_i is an independent random variable following a uniform distribution on $[0, 1]$. The randomized version of NNM requires only a slight modification to the original method: the nearest neighbor is still matched using the no-random score, but the same random factor is applied during the computation process. Specifically, it can be expressed as:

$$\tilde{S}_{\text{nnm-r}}(\tilde{\mathbf{x}}_i, \mathcal{D}_{\text{labeled}}, S, f, u_i) = S(\tilde{\mathbf{x}}_i, \hat{y}, u_i) + S(\mathbf{x}_j, y_j, u_i) - S(\mathbf{x}_j, \hat{y}, u_i),$$

$$\text{where } j = \arg \min_{j \in \{1, \dots, n\}} |S(\tilde{\mathbf{x}}_i, \hat{y}) - S(\mathbf{x}_j, \hat{y})|.$$

Here, u_i remains independent of (\mathbf{x}_i, y_i) , but the same u_i in $S(\cdot)$ is used for each $\tilde{\mathbf{x}}_i$. The experimental results for NNM-R are presented in Appendix H.8.

F Supplemental algorithms

The complete algorithm flow of SemiCP and its variant, SemiCP-conditional, is as follows.

Algorithm 1 SemiCP: Semi-supervised Conformal Prediction

Require: Labeled data $\mathcal{D}_{\text{labeled}} = \{(\mathbf{x}_i, y_i)\}_{i=1}^n$, Unlabeled data $\mathcal{D}_{\text{unlabeled}} = \{\tilde{\mathbf{x}}_i\}_{i=1}^N$, Significance level $\alpha \in (0, 1)$, Score function $S(\cdot, \cdot)$, Prediction model $f(\cdot)$, Test input \mathbf{x}_{test} , Label set \mathcal{Y}

Ensure: Prediction set $\mathcal{C}_{\text{SemiCP}}(\mathbf{x}_{\text{test}})$

- 1: Compute nonconformity scores for labeled data: $s_i = S(\mathbf{x}_i, y_i)$, $i = 1, \dots, n$
 - 2: Estimate nonconformity scores \tilde{s}_i for unlabeled data $\tilde{\mathbf{x}}_i$:
 - 3: **for** $i = 1$ **to** N **do**
 - 4: $j = \arg \min_{j \in \{1, \dots, n\}} |S(\tilde{\mathbf{x}}_i, \hat{y}) - S(\mathbf{x}_j, \hat{y})|$
 - 5: $\tilde{s}_i = S(\tilde{\mathbf{x}}_i, \hat{y}) + S(\mathbf{x}_j, y_j) - S(\mathbf{x}_j, \hat{y})$
 - 6: **end for**
 - 7: Compute threshold: $\hat{\tau}_{\text{SemiCP}} = \text{Quantile} \left(\{s_i\}_{i=1}^n \cup \{\tilde{s}_i\}_{i=1}^N, \frac{\lceil (n+N+1)(1-\alpha) \rceil}{n+N} \right)$
 - 8: Form prediction set: $\mathcal{C}_{\text{SemiCP}}(\mathbf{x}_{\text{test}}) = \{y \in \mathcal{Y} : S(\mathbf{x}_{\text{test}}, y) \leq \hat{\tau}_{\text{SemiCP}}\}$
 - 9: **return** $\mathcal{C}_{\text{SemiCP}}(\mathbf{x}_{\text{test}})$
-

G Evaluation metrics

AvgSize (Average Prediction Set Size) The average prediction set size quantifies the mean number of labels in the prediction sets:

$$\text{AvgSize} = \frac{1}{|\mathcal{D}_{\text{test}}|} \sum_{(\mathbf{x}, y) \in \mathcal{D}_{\text{test}}} |\mathcal{C}(\mathbf{x})|.$$

Algorithm 2 SemiCP-conditional: Semi-supervised Conformal Prediction on conditional setting

Require: Labeled data $\mathcal{D}_{\text{labeled}} = \{(\mathbf{x}_i, y_i)\}_{i=1}^n$, Unlabeled data $\mathcal{D}_{\text{unlabeled}} = \{\tilde{\mathbf{x}}_i\}_{i=1}^N$, Significance level $\alpha \in (0, 1)$, Score function $S(\cdot, \cdot)$, Prediction model $f(\cdot)$, Test input \mathbf{x}_{test} , Label set \mathcal{Y} , Group set \mathcal{G}

Ensure: Prediction set $\mathcal{C}_{\text{SemiCP}}(\mathbf{x}_{\text{test}})$

- 1: Compute nonconformity scores for labeled data: $s_i = S(\mathbf{x}_i, y_i)$, $i = 1, \dots, n$
 - 2: Estimate nonconformity scores \tilde{s}_i for unlabeled data $\tilde{\mathbf{x}}_i$:
 - 3: **for** $i \in \{1, \dots, N\}$ **do**
 - 4: $j = \arg \min_{j \in \{1, \dots, n\}} |S(\tilde{\mathbf{x}}_i, \hat{y}) - S(\mathbf{x}_j, \hat{y})|$
 - 5: $\tilde{s}_i = S(\tilde{\mathbf{x}}_i, \hat{y}) + S(\mathbf{x}_j, y_j) - S(\mathbf{x}_j, \hat{y})$
 - 6: **end for**
 - 7: **for** $G_i \in \mathcal{G}$ **do**
 - 8: Select all nonconformity scores belonging to group G_i : $\{s_i\}_{i=1}^{n_g}, \{\tilde{s}_i\}_{i=1}^{N_g}$
 - 9: Compute threshold: $\hat{\tau}_{\text{SemiCP}}^g = \text{Quantile}\left(\{s_i\}_{i=1}^{n_g} \cup \{\tilde{s}_i\}_{i=1}^{N_g}, \frac{[(n_g + N_g + 1)(1 - \alpha)]}{n_g + N_g}\right)$
 - 10: **end for**
 - 11: Form prediction set: $\mathcal{C}_{\text{SemiCP}}(\mathbf{x}_{\text{test}} \in G_i) = \{y \in \mathcal{Y} : S(\mathbf{x}_{\text{test}}, y) \leq \hat{\tau}_{\text{SemiCP}}^g\}$
 - 12: **return** $\mathcal{C}_{\text{SemiCP}}(\mathbf{x}_{\text{test}})$
-

CovGap (Average Coverage Gap) Coverage gap measures how far the marginal coverage deviates from the desired coverage level of $1 - \alpha$. The marginal coverage is defined as $\hat{c} = \frac{1}{|\mathcal{D}_{\text{test}}|} \sum_{(\mathbf{x}, y) \in \mathcal{D}_{\text{test}}} \mathbb{I}_{y \in \mathcal{C}(\mathbf{x})}$, then the average coverage gap is given by:

$$\text{CovGap} = 100 \times |\hat{c} - (1 - \alpha)|.$$

For conditional conformal prediction, coverage gap evaluates the deviation of each subgroup's coverage from the target coverage $1 - \alpha$. For example, in class-conditional conformal prediction, let $\mathcal{J}^y = \{i \in [N'] : Y'_i = y\}$ denote the index set of samples with label y . The coverage for class y is defined as: $\hat{c}_y = \frac{1}{|\mathcal{J}^y|} \sum_{i \in \mathcal{J}^y} \mathbb{I}_{y'_i \in \mathcal{C}(\mathbf{x}'_i)}$, then the class-conditional coverage gap is given by:

$$\text{CovGap} = 100 \times \frac{1}{|\mathcal{Y}|} \sum_{y \in \mathcal{Y}} |\hat{c}_y - (1 - \alpha)|.$$

Improvement Throughout the paper, "improvement" refers to the relative performance gain of a method over a baseline. Suppose M denotes the evaluation metric of interest, the improvement is computed as:

$$\text{improvement} = \frac{M_{\text{Standard}} - M_{\text{SemiCP}}}{M_{\text{Standard}} - M_{\text{Oracle}}} \times 100\%.$$

OverCovGap and UnderCovGap In section H.1, we also report Over-Coverage Gap and Under-Coverage Gap metrics to avoid the potential masking effect of the overall coverage gap, which may conceal the disadvantage of under-coverage. The Over-Coverage Gap and Under-Coverage Gap are defined as:

$$\begin{aligned} \text{OverCovGap} &= 100 \times \mathbb{I}\{\hat{c} > (1 - \alpha)\} \cdot |\hat{c} - (1 - \alpha)|, \\ \text{UnderCovGap} &= 100 \times \mathbb{I}\{\hat{c} < (1 - \alpha)\} \cdot |\hat{c} - (1 - \alpha)|. \end{aligned}$$

H Supplemental experiments

H.1 Supplemental metrics with OverCovGap and UnderCovGap metrics

Since the CovGap metric may obscure the separate effects of over-coverage and under-coverage, we additionally measure the over-coverage and under-coverage of our method, SemiCP, denoted as OverCovGap and UnderCovGap (see Appendix G). Figure 8 illustrates the extent to which SemiCP improves over-coverage and under-coverage compared to the standard method under varying amounts of labeled data. The results demonstrate that our method consistently achieves lower levels of both over-coverage and under-coverage, suggesting a robust improvement over the standard method.

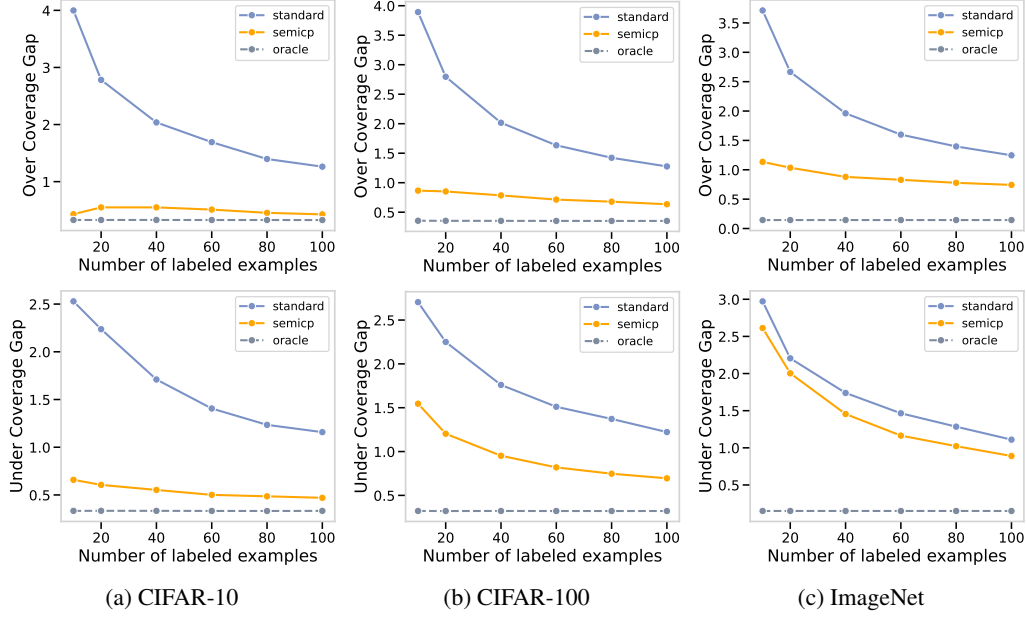


Figure 8: Comparison of the relationship between Over Coverage Gap (top) and Under Coverage Gap (bottom) with different label data numbers. Experiments conducted on CIFAR-10, CIFAR-100, and ImageNet datasets using ResNet50, average on three score functions with 1000 different trials.

H.2 SemiCP is compatible with various score functions

Table 2 summarizes the performance of our approach under three different score functions—THR, APS, and RAPS—across CIFAR10, CIFAR100, and ImageNet. The results reveal that SemiCP consistently narrows the coverage gap and reduces the average set size, regardless of the labeled score employed. For instance, SemiCP reduces 81.89% coverage gap and 97.32% set sizes for APS, while its performance nearly matches that of the oracle method. Similar trends are observed on THR and RAPS, where SemiCP shows substantial improvements. Notably, SemiCP is more effective for those scores that initially yield poorer performance. Specifically, the improvement in APS is greater than that in RAPS, which in turn exceeds the improvement observed with THR. These improvements confirm the compatibility of SemiCP across different labeled score functions.

Table 2: Average coverage gap and set size with different score functions on three datasets. Standard errors are reported in parentheses. The number of labeled data is fixed at 80.

Score		THR		APS		RAPS	
Dataset	Method	CovGap	AvgSize	CovGap	AvgSize	CovGap	AvgSize
CIFAR10	standard	2.64 (2.0)	0.91 (0.0)	2.62 (1.9)	1.44 (0.1)	2.63 (1.9)	1.40 (0.1)
	semicp	0.88 (0.8)	0.90 (0.0)	0.96 (0.8)	1.42 (0.0)	0.98 (0.8)	1.38 (0.0)
	oracle	0.65 (0.5)	0.90 (0.0)	0.66 (0.5)	1.42 (0.0)	0.66 (0.5)	1.38 (0.0)
CIFAR100	standard	2.68 (2.0)	1.21 (0.2)	2.88 (2.1)	39.40 (5.2)	2.83 (2.1)	11.02 (0.9)
	semicp	2.57 (1.8)	1.19 (0.3)	0.75 (0.6)	38.56 (1.2)	0.95 (0.8)	10.92 (0.3)
	oracle	0.69 (0.5)	1.15 (0.0)	0.67 (0.5)	38.57 (0.9)	0.67 (0.5)	10.93 (0.2)
ImageNet	standard	2.69 (2.0)	1.70 (0.5)	2.66 (2.0)	179.35 (51.2)	2.70 (2.0)	16.57 (3.4)
	semicp	2.63 (1.9)	1.62 (0.5)	1.13 (0.8)	166.98 (22.3)	1.64 (1.2)	15.90 (2.3)
	oracle	0.29 (0.2)	1.52 (0.0)	0.30 (0.2)	166.15 (2.7)	0.29 (0.2)	15.74 (0.2)
improvement		32.26%	55.43%	81.89%	97.32%	71.51%	96.11%

H.3 Effect of pseudo-label quality on SemiCP performance

SemiCP relies on labeled data selected via pseudo-label uncertainty, making pseudo-label quality a critical factor. We quantify this quality by the Top-1 accuracy of the pseudo-labeling model. As shown in Figure 9, when accuracy is low, SemiCP performs similarly to the standard baseline. As accuracy increases, the coverage gap steadily decreases and drops sharply beyond 90%, approaching zero. The average set size remains stable initially, then declines significantly with higher accuracy. These results indicate that even moderate pseudo-label quality suffices to improve calibration over standard CP, demonstrating the robustness and practical viability of SemiCP in semi-supervised settings.

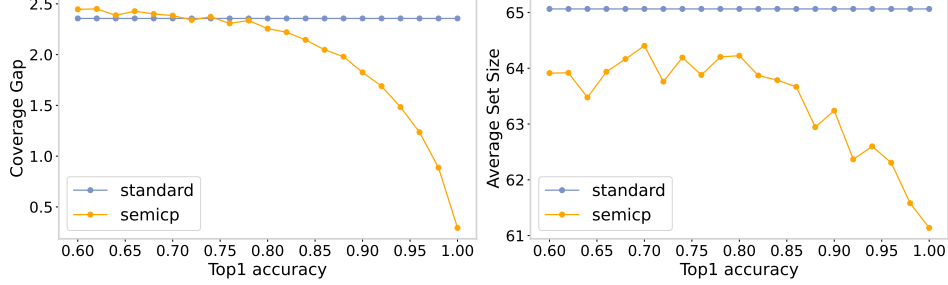


Figure 9: Coverage gap and average set size of SemiCP with different pseudo-label accuracies. Each experiment was conducted on ImageNet and averaged over three score functions with 1000 trials. The number of labeled data and unlabeled data is fixed at 100 and 20000.

H.4 Robustness to labeled data distribution shift

In real-world applications, the exchangeability assumption in conformal prediction often fails when labeled calibration data shift. To assess SemiCP’s robustness, we test it with labeled data from a shifted domain (ImageNet-R(Kornblith et al., 2019)/ImageNet-S(Gao et al., 2022)/ImageNet-V2(Recht et al., 2019)), while the unlabeled and test data follow the target distribution. As shown in Table 3, SemiCP consistently outperforms standard CP in mitigating distribution shift, reducing the coverage gap by 8.35%–49.83% and prediction set size by 3.14%–53.14%, demonstrating its ability to recalibrate decision boundaries with target domain unlabeled data, even when labeled data is biased.

Table 3: Comparison of CovGap and AvgSize across different distribution shift scenarios. Each experiment was conducted on ImageNet and averaged over three score functions with 100 trials. The number of labeled data and unlabeled data is fixed at 20 and 20000.

Method	ImageNet-R		ImageNet-S		ImageNetV2	
	CovGap	AvgSize	CovGap	AvgSize	CovGap	AvgSize
standard	9.40 (1.1)	546.85 (198.6)	4.85 (3.9)	74.73 (110.4)	5.82 (3.9)	91.18 (129.6)
semicp	8.64 (2.1)	498.33 (358.9)	3.07 (2.7)	74.31 (132.5)	3.06 (2.3)	75.24 (114.9)
oracle	0.29 (0.2)	61.19 (74.6)	0.29 (0.2)	61.19 (74.7)	0.29 (0.2)	61.19 (74.7)
improvement	8.35%	9.99%	38.88%	3.14%	49.83%	53.14%

H.5 Discussion of different bias estimation methods

Figure 10 compares four bias estimators. The *naive* method ignores the gap between the true nonconformity score $S(\mathbf{x}_j, y_j)$ and the pseudo-label score $S(\mathbf{x}_j, \hat{y}_j)$. The *debias* estimator corrects this by using the average bias of all labeled data, $\text{Bias} = \frac{1}{n} \sum_{j=1}^n [S(\mathbf{x}_j, y_j) - S(\mathbf{x}_j, \hat{y}_j)]$. In *random-sample*, we assign each unlabeled example the bias of a randomly chosen labeled point. Our *semicp* estimator is defined in Equation 4.

The left panel shows that *semicp* steadily reduces the coverage gap as the number of labeled samples n increases, outperforming the standard CP baseline at all n . The other methods yield modest gains at very small n (e.g. $n = 10$) but quickly degrade relative to the baseline. The right panel plots prediction-set size: *random-sample* always produces overly large sets, *debias* performs well initially but worsens with growing n , and *naive* underestimates scores—hence thresholds—and fails to guarantee coverage (see Section 3.2). Detailed theory of four estimators is deferred to Section C. Overall, *semicp* offers the best balance of reliability and efficiency.

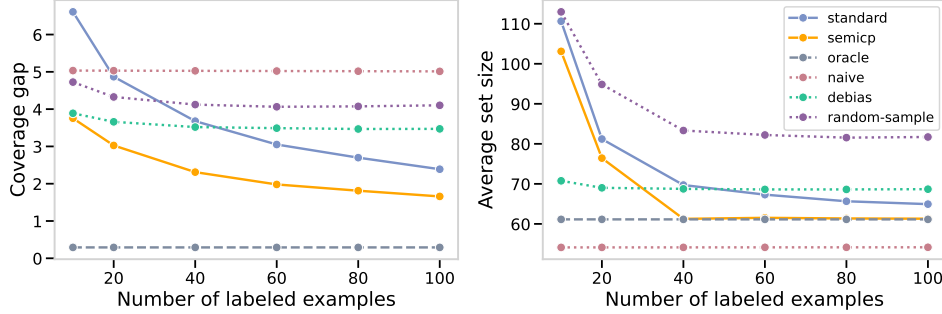


Figure 10: Average Coverage Gap and Set Size of SemiCP with different bias estimation methods. Each experiment was conducted on ImageNet and ResNet50, averaged over three score functions with 1000 trials. The number of unlabeled data is fixed at 20000.

H.6 Ablation study of different neighborhood selection methods

In Figure 11, we compare several neighborhood selection criteria as an ablation study. Our proposed method, *nnm*, matches a labeled example with the most similar nonconformity score with a pseudo-label. In addition, *nearest_confidence* selects labeled examples with the highest model confidence; *nearest_score* finds the neighbor whose full nonconformity-score vector $S(\tilde{x})$ is most similar; *nearest_logit* matches on the raw logit outputs of the model for x ; and *nearest_feature* uses the input-feature embedding for matching. All high-dimensional distances are measured with the Euclidean metric.

On the coverage gap metric (left), *nnm* uniformly outperforms the competing methods. On average set size (right), *nearest_confidence* and *nearest_score* slightly undercut *nnm* at $n = 10$, but as the number of labeled examples increases, our method *nnm* exhibits a clear and sustained advantage. For example, at $n = 60$, *nnm* reduces the average set size from 69 to 61, whereas all alternative methods fail to improve upon the standard baseline. Overall, these results confirm that our neighborhood-selection criterion is optimal, yielding the most reliable coverage guarantees and the smallest prediction sets.

H.7 Ablation study of different numbers of neighborhood

In Figure 12, we present the results of SemiCP with different numbers of nearest neighbors. In the figure, *nnm_k* denotes the number of nearest neighbors chosen, where k indicates the number of neighbors. When multiple neighbors are selected, the bias $\Delta(\tilde{x}_i)$ is estimated as the average of the biases of the k nearest neighbors, i.e., $\frac{1}{k} \sum_{i=1}^k \Delta(x_j)$. The left plot shows that with $k = 1$, the coverage gap is minimized, achieving a more stable coverage of $1 - \alpha$. On the right, although the set size for $k = 2, 3, 5$ is even smaller than that of the oracle, this suggests that the coverage may not have been guaranteed, leading to overly small prediction sets. This could be because selecting closer neighbors allows for more accurate distribution estimates, resulting in better performance.

H.8 SemiCP for nonconformity score with random factor

Table 4 compares the performance of SemiCP under nonrandom and randomized matching strategies. Both versions consistently outperform the standard method in terms of reducing coverage gap across datasets and settings, confirming the effectiveness of leveraging unlabeled data. The non-random variant achieves the lowest coverage gap, indicating that deterministic matching yields more accurate bias correction. In contrast, the randomized version produces smaller average set sizes, particularly

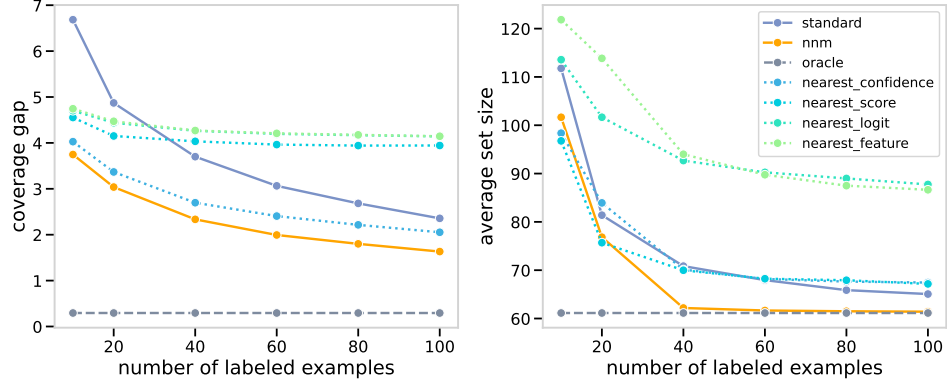


Figure 11: Average Coverage Gap and Set Size of SemiCP with different neighborhood selection methods. Each experiment was conducted on ImageNet and ResNet50, averaged over three score functions with 1000 trials. The number of unlabeled data is fixed at 20000.

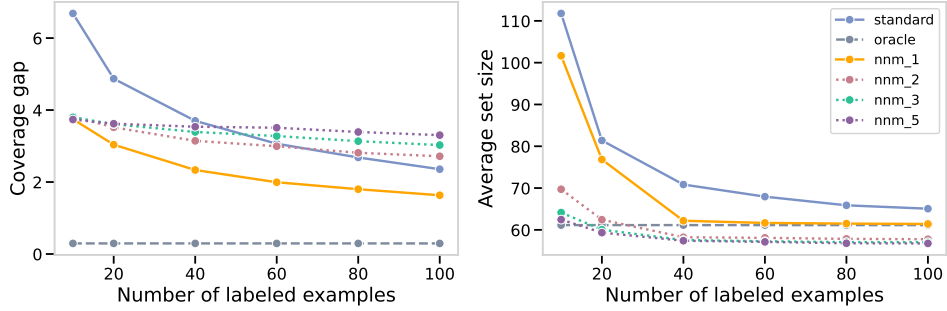


Figure 12: Coverage gap and average set size of SemiCP with different neighborhood numbers. Each experiment was conducted on ImageNet and averaged over three score functions with 1000 trials. The number of unlabeled data is fixed at 20000.

on high-class datasets such as CIFAR100 and ImageNet. This reflects a trade-off: the random strategy sacrifices a small amount of coverage for improved compactness, which may be desirable in scenarios with large output spaces or limited labeling budgets.

Table 4: Average coverage gap and set size with different score functions, no random and random versions on three datasets. The number of labeled data is fixed at 100.

n	Score		APS(no random)		APS(random)		RAPS(no random)		RAPS(random)	
	Dataset	Method	CovGap	AvgSize	CovGap	AvgSize	CovGap	AvgSize	CovGap	AvgSize
10	CIFAR10	standard	6.59	1.94	6.97	1.34	6.59	1.83	6.97	1.33
		semicp	1.23	1.42	1.82	0.97	1.29	1.38	1.83	0.96
		oracle	0.67	1.41	0.67	0.96	0.66	1.38	0.67	0.96
	CIFAR100	standard	6.04	46.91	7.82	15.01	6.13	12.64	7.67	6.71
		semicp	0.77	38.74	2.75	8.26	1.1	11.11	3.24	4.43
		oracle	0.63	38.62	0.69	8.01	0.6	10.94	0.68	4.22
	ImageNet	standard	6.45	273.48	6.23	117.55	6.35	28.9	6.21	21.95
		semicp	1.46	157.77	4.21	40.13	3.04	16.2	4.83	7.8
		oracle	0.3	166.26	0.31	36.89	0.26	15.76	0.32	6.53
20	CIFAR10	standard	5.17	1.53	4.93	1.00	5.17	1.46	4.93	0.99
		semicp	1.12	1.41	1.66	0.96	1.17	1.38	1.67	0.95
		oracle	0.67	1.41	0.66	0.96	0.65	1.38	0.66	0.96
	CIFAR100	standard	4.85	43.48	5.04	11.37	4.80	11.59	4.89	5.04
		semicp	0.70	38.49	2.34	7.82	0.98	10.89	2.62	4.11
		oracle	0.62	38.63	0.67	7.98	0.60	10.94	0.67	4.21
	ImageNet	standard	4.25	219.51	4.88	67.95	4.46	20.03	4.65	11.14
		semicp	1.45	161.03	3.39	39.63	2.46	15.75	3.79	7.16
		oracle	0.30	166.26	0.30	36.82	0.26	15.76	0.31	6.53
50	CIFAR10	standard	3.62	1.49	3.42	0.97	3.60	1.44	3.42	0.97
		semicp	1.17	1.43	1.51	0.96	1.21	1.39	1.52	0.96
		oracle	0.67	1.41	0.65	0.96	0.66	1.38	0.65	0.96
	CIFAR100	standard	3.84	39.96	3.59	9.57	3.81	11.07	3.55	4.67
		semicp	0.71	38.59	1.82	8.31	1.00	10.93	1.99	4.32
		oracle	0.62	38.61	0.66	7.99	0.61	10.94	0.66	4.21
	ImageNet	standard	3.53	186.92	3.49	52.32	3.52	17.13	3.36	8.13
		semicp	1.35	165.10	2.42	43.15	2.03	15.95	2.73	7.36
		oracle	0.30	166.25	0.32	36.68	0.26	15.76	0.30	6.51
100	CIFAR10	standard	2.37	1.44	2.23	0.97	2.36	1.40	2.25	0.97
		semicp	0.99	1.42	1.23	0.96	1.00	1.38	1.23	0.96
		oracle	0.67	1.41	0.65	0.96	0.66	1.38	0.64	0.96
	CIFAR100	standard	2.84	38.96	2.48	9.01	2.74	10.96	2.35	4.51
		semicp	0.76	38.64	1.44	8.20	0.93	10.93	1.49	4.24
		oracle	0.63	38.63	0.66	8.04	0.61	10.94	0.68	4.23
	ImageNet	standard	2.74	172.76	2.41	41.71	2.71	16.24	2.33	7.00
		semicp	1.05	163.38	1.90	39.05	1.50	15.77	2.17	6.86
		oracle	0.30	166.23	0.31	36.73	0.27	15.76	0.31	6.52
improvement			85.03%	100.55%	55.48%	88.4%	74.26%	101.64%	48.69%	88.69%